European Radiology (2019) 29:5423–5430
https://doi.org/10.1007/s00330-019-06149-0

ONCOLOGY

Morphological classification of pre-invasive lesions and early-stage lung adenocarcinoma based on CT images

Feng Gao[1] · Ming Li[1,2,3] · Ziwei Zhang[4] · Li Xiao[5] · Guozhen Zhang[1] · Xiangpeng Zheng[2] · Yanqing Hua[1] · Jianying Li[6]

Received: 18 September 2018 / Revised: 18 February 2019 / Accepted: 8 March 2019 / Published online: 22 March 2019

Abstract

Objective To retrospectively analyze the computed tomography (CT) features in patients with pre-invasive lesions and early-stage lung adenocarcinoma and to explore the correlation between tumor morphological changes and pathological diagnoses.

Materials and methods CT morphological characteristics in 2106 patients with pre-invasive (stage 0) and early-stage (stage I) lung adenocarcinoma were analyzed; lesions were confirmed by surgical pathology. Based on the morphological characteristics, the lesions were divided into eight types: I (cotton ball, ground-glass nodules), II (solid fill), III (granular), IV (dendriform), V (bubble-like lucencies), VI (alveolate or honeycomb), VII (scar-like), and VIII (notched or umbilication). The different distributions of eight morphological types in pathological types of the lesions and subtypes of invasive adenocarcinoma were analyzed by *chi-squared* or *Fisher's* exact test. Correlation between the percentage of ground-glass opacity in the lesions and pathology types were analyzed by two-tailed *Pearson's* test.

Results A negative correlation was observed between the pathological types and proportion of ground-glass component in the lesions ($p < 0.001$ and $r = -0.583$). Significant differences in morphological characteristics among various pathological types of pre-invasive lesions and early lung adenocarcinomas were observed ($p < 0.05$). Furthermore, among the different pathological subtypes of stage I invasive adenocarcinoma, the differences in their manifestation as morphological types I, II, III, and VI were statistically significant ($p < 0.05$).

Conclusion The eight types of morphological classification of pre-invasive lesions and early-stage (stage 0 or stage I) lung adenocarcinoma has different pathological bases, and morphological classification may be useful for the diagnosis and differential diagnosis of lung adenocarcinoma.

Key Points

- *CT morphological classification of pre-invasive lesions and lung adenocarcinoma is intuitive.*
- *CT morphological classification characterizes morphological changes of the entire lesion.*
- *Different pathological types of lung adenocarcinoma have different morphological features.*

Keywords Lung adenocarcinoma · Morphological · Computed tomography

Electronic supplementary material The online version of this article (https://doi.org/10.1007/s00330-019-06149-0) contains supplementary material, which is available to authorized users.

✉ Ming Li
minli77@163.com

[1] Department of Radiology, Huadong Hospital Fudan University, Shanghai 200040, China

[2] Diagnostic and Treatment Center of Small Lung Nodules, Huadong Hospital Fudan University, 221#, West Yanan Road, Shanghai 200040, China

[3] Institute of Functional and Molecular Medical Imaging, Fudan University, Shanghai 200040, China

[4] Department of Radiology, Duke University Medical Center, Durham, NC, USA

[5] Department of Pathology, Huadong Hospital Fudan University, Shanghai 200040, China

[6] CT Research Center, GE Healthcare China, Shanghai 200040, China

Abbreviations

AAH	Atypical adenomatous hyperplasia
AIS	Adenocarcinoma in situ
CPR	Curved planar reformation
GGN	Ground-glass nodule
GGO	Ground-glass opacity
IAC	Invasive adenocarcinoma
LLL	Left lower lobe
LUL	Left upper lobe
mGGN	Mixed ground-glass nodule
MIA	Minimal invasive adenocarcinoma
MIP	Maximum intensity projection
MPR	Multi-planar reformation
pGGN	Pure ground-glass nodule
RLL	Right lower lobe
RML	Right middle lobe
RUL	Right upper lobe
VR	Volume rendering

Introduction

Lung cancer is one of the most common cancers in both men and women, as well as a leading cause of cancer-related death worldwide [1]. Lung adenocarcinoma is the most common subtype of lung cancer [2]. In clinical practice, preoperative diagnosis is mainly the basis on the lesions' morphological features on CT images, such as density, border, and the relationship with surrounding structures [3–5]. Morphological features are more obvious in tumors of larger sizes and volumes. In addition, previous studies about the morphological features are mainly focused on the local changes of lesions [3, 6]. In this study, morphological changes of tumors were divided into eight types, and typical CT images and their mode pictures corresponding to these different morphological types were identified through training, and pre-invasive lesions (stage 0) and early-stage (stage I) lung adenocarcinoma were classified based on their CT appearances. A total of 2106 patients with stage 0 and stage I lung adenocarcinoma were included in this study to explore the correlation between tumor morphological changes and pathological diagnoses.

Materials and methods

Patients

This study was a retrospective analysis. A total of 2106 pre-invasive lesions (stage 0) and early-stage (stage I) lung adenocarcinoma which were surgically resected between January 2012 and December 2017 in our hospital were included in this study, based on the following criteria: (a) patients had no history of malignant tumor and (b) single solitary lesion in the lungs. The exclusion criteria were as follows: (a) patients with multiple pulmonary lesions were excluded from the study, because it was hard to confirm whether the lesions were metastatic or multiple primary neoplasms; (b) the pathological diagnosis was not lung adenocarcinoma or the TNM staging result was not a pre-invasive (stage 0) or early-stage (stage I) lesion; and (c) patients with surgery more than 2 weeks after CT examination were excluded. Tumor staging was surgically confirmed with reference to the 8th Edition of the TNM Classification for Lung Cancer [7]. For the patients who were admitted into hospital when the 7th TNM was still in use, their cases were restaged according to the 8th edition.

There were 740 males and 1366 females, ranging between 22 and 85 years in age (average age of 57.18 ± 11.97 years old).

CT scan protocol and image reformations

Chest CT imaging (field-of-view from the apex to the lung basis, including the chest wall and axilla) was performed on a 64-detector CT system (GE Light speed VCT or GE Discovery CT750 HD, GE Healthcare) using the following protocol parameters: 1.25-mm slice thickness with a 1.25-mm reconstruction interval, pitch of 0.984, 120 kV, and 250 mA, and bone reconstruction kernel. All images were reviewed with a high-resolution 52.8-cm, 2048 × 1560-pixel grayscale monitor with a standard lung window (window width, 1500 HU; window level, − 500 HU) and a mediastinal window (window width, 350 HU; window level, 50 HU). All lesions were subject to conventional 3D post-processing, including maximum intensity projection (MIP), multiple planar reformation (MPR), volume rendering (VR), and curved planar reformation (CPR).

Pathological diagnosis

The pathological diagnosis and categorization of atypical adenomatous hyperplasia (AAH), adenocarcinoma in situ (AIS), MIA, and IAC were made based on the new pulmonary adenocarcinoma classification, 2011 edition [8]. Although some patients had undergone biopsy before surgery, the final pathological diagnoses were based on the surgical specimen. Two senior pathologists (with more than 20 years of pathological diagnosis experience) performed all histological preparations and analyses. Any disagreement was discussed and resolved by a mutual consensus or after consultation with a third pathologist.

Nodule evaluation

Ground-glass nodule (GGN) lesion is defined as a hazily increased attenuation in the lung with preservation of intact bronchial and vascular structures [9–11]. GGNs are further subdivided into mixed GGNs (mGGNs) and pure GGNs (pGGNs) [12]. For mixed ground-glass nodule (mGGN) and solid nodule, the solid components were measured using a

standard lung window (window width, 1500 HU; window level, − 500 HU); the size of the lesion was defined as the average value of long and short axial diameters and craniocaudal height; the percentage of the ground-glass opacity (GGO) component was calculated according to the following formula: $([D_{GGO}-D]) / D_{GGO} \times 100$, where D_{GGO} is the largest diameter of the entire lesion, and D is the largest diameter of the solid component (excluding vessels) within the lesion [12].

CT morphological classifications were divided into eight types (Figs. 1 and 2): Type I (cotton ball), round or oval nodules, pure GGN (pGGN) or mGGN, which appears as cotton balls. Type II (solid fill), round or oval solid density nodules; in some cases, the lesions are mGGNs with a solid peripheral rim and a low-density or ground-glass density center. Type III (granular), the lesions are mostly mGGN, with dispersed spots or granular solid components in GGO background. Type IV (dendriform), the lesions or the lesion boundaries show tree branch-like morphology: a main trunk with multiple smaller branches; the long axis of the lesion spreading in the same direction with the bronchi; GGNs or solid lesions. Type V (bubble-like lucencies), a single air density vacuole or cavity surrounded by a GGO, solid or part-solid rim. Type VI (honeycomb), the lesion has vacuole sign and/or dilated bronchus, giving the lesion a tiny bubbly or honeycomb-like morphology. Type VII (scar-like), the lesions are secondary lung adenocarcinomas derived from primary fibrous scars or old tuberculosis lesions; such lesions were previously referred to as "scar cancers" [13]. Type VIII (notched or umbilication), the lesions are usually abutting or near the interlobar fissures, and the pleura can shift toward the lesions, resulting in a C-, V-, or Y-shape.

Nodule evaluation was performed by two senior radiologists, with more than 35 and 20 years of radiological diagnosis experience, respectively. They first observed and discussed the typical CT images and their mode pictures corresponding to eight different morphological types. Then, they classified the lesions without knowing their pathological diagnoses. Any disagreement was resolved with a consensus after discussion.

Statistics analysis

Statistical analyses were performed with a commercially available computer software program (SPSS v. 17.0 for Windows, SPSS). Counting data were examined using the *chi-squared* test, and *Fisher's* exact test was employed to examine the probability when the expected value in one or more cells was < 5. The

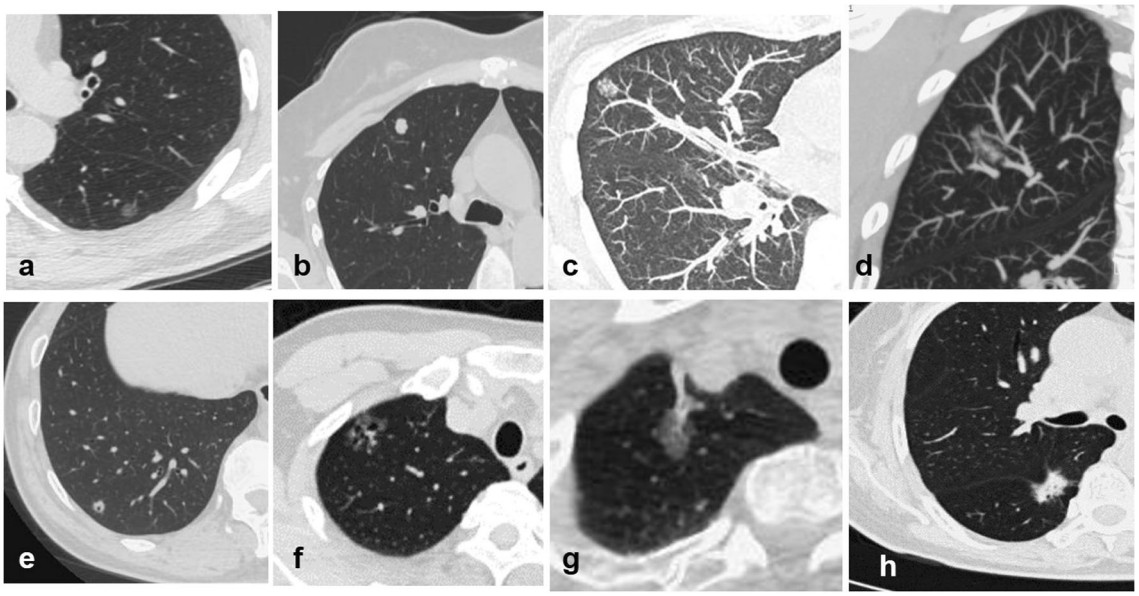

Fig. 1 **a** Type I (cotton ball), axial images showing a pGGN located in the LLL. The lesion was resected and confirmed to be a lepidic predominant IAC by pathology. **b** Type II (solid fill), axial images showing a solid nodule located in the RUL. The lesion was resected and confirmed to be a lepidic predominant IAC by pathology. **c** Type III (granular), an mGGN in the RML, axial MIP image showing some solid particles within the lesion. The lesion was resected and confirmed to be a micropapillary predominant IAC by pathological examination. **d** Type IV (dendriform), coronal MIP image showing a mGGN in the RUL and developing along the longitudinal axis of the bronchovascular bundle. The lesion was resected and confirmed to be a papillary predominant IAC by pathology. **e** Type V (bubble-like lucencies), axial image showing solid nodule in the RLL, with a bubble-like lucency area located centrally within the lesion. The lesion was resected and confirmed to be a mucinous predominant IAC by pathology. **f** Type VI (honeycomb), axial CT image showing a mGGN in the RUL, with multiple small air spaces within the lesion. The lesion was resected and confirmed to be a papillary predominant IAC by pathology. **g** Type VII (scar-like), axial image showing fibrous lesion enlargement and well-defined GGO emerging around the previously existing fibrous lesion. The lesion was resected and confirmed to be a micropapillary predominant IAC by pathology. **h** Type VIII (notched or umbilication), axial CT image showing a mGGN in RLL and connected with a major fissure causing displacement of a related fissure. The lesion was resected and confirmed to be an acinar predominant IAC by pathology

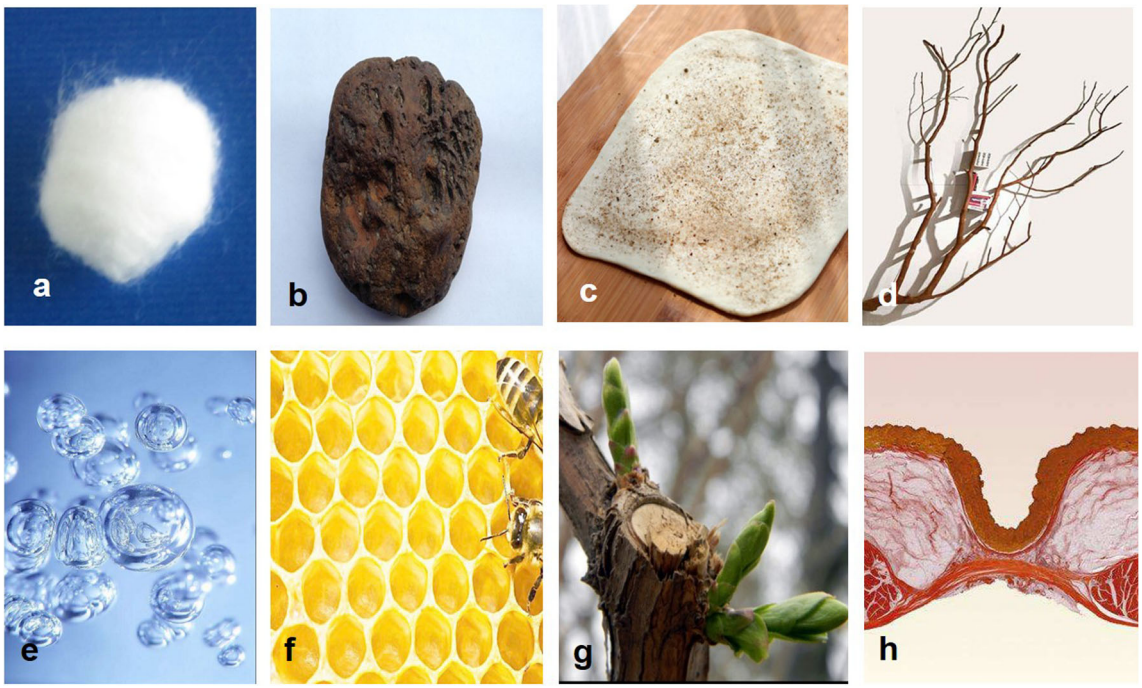

Fig. 2 The modular picture of different types. **a** Type I (cotton ball). **b** Type II (solid fill). **c** Type III (granular). **d** Type IV (dendriform). **e** Type V (bubble-like lucencies). **f** Type VI (honeycomb). **g** Type VII (scar-like). **h** Type VIII (notched or umbilication)

different distributions of eight morphological types in four different pathological types of early-stage (stage 0 or stage I) adenocarcinoma and in six different subtypes of invasive adenocarcinoma were analyzed by *Chi-squared* test or *Fisher's* exact test. Quantitative data were expressed as the mean ± standard deviation. Correlational analyses were conducted between the percentage of ground-glass opacity in the lesions and pathology types, using two-tailed *Pearson's* test. $P < 0.05$ was considered statistically significant (the p value was recalibrated accordingly in pairwise comparisons).

Results

The clinical characteristics and pathological classification are shown in Table 1. Lesion sizes and percentages of GGO components are presented in Table 2. There was a significant negative correlation between GGO components and the pathological types ($p < 0.001$, $r = -0.583$). From AAH, AIS to MIA and IAC, the percentages of GGO components in the nodule gradually decreased.

Morphological classifications of early-stage (stage 0 or stage I) lung adenocarcinomas were shown in Table 3. Among different pathological types of early-stage (stage 0 or stage I) lung adenocarcinoma, there were significant differences in the number of cases with different morphological types ($p < 0.001$). There were significant differences in the number of cases among preinvasive lesions and IAC, MIA and IAC, but there were no significant differences in the number of cases between preinvasive lesions and MIA (Supplementary Table 1). Cotton ball–like type I morphology was observed in AAH (100%), AIS (88.03%), MIA (85.09%), and IAC (43.06%). In AIS lesions, 16 (6.84%) cases were type II, while seven cases were mucinous subtype. All the other 227 cases of AIS were nonmucinous subtype. In MIA, 54 (6.6%) cases were type II, while a low percentage of other morphological types were also observed. Among IAC lesions, 204 (20.52%) cases showed type II solid fill lesions; all other morphological types were observed and were almost evenly distributed.

Morphological classification of different subtypes of invasive adenocarcinomas is shown in Table 4. Among pathological subtypes of stage I invasive adenocarcinoma, most (78.27%, 778/994) of the included cases were acinar predominant subtype. Among different pathological subtypes of invasive adenocarcinoma, there were significant differences in the number of cases with different morphological types ($p < 0.001$). There were no significant differences in the number of cases among acinar and lepidic predominant invasive adenocarcinoma, acinar predominant and mucinous adenocarcinoma, micropapillary predominant and mucinous adenocarcinoma, and solid predominant and mucinous adenocarcinoma, but there were significant differences in the number of cases among other subtypes' pairwise comparisons (Supplementary Table 2). Type I was observed in 45.0% of acinar predominant invasive adenocarcinoma cases followed by type II (18.00%), while the remaining ones represented other types which were evenly distributed. For the lepidic predominant invasive adenocarcinoma, 60.71% were type I, 20.52% were type II, and 14.29% cases were type III. For the

Table 1 Clinical characteristics of patients with pre-invasive lesion and early-stage (stage 0 or stage I) lung adenocarcinomas

Characteristics	Overall ($n = 2106$, %)
Sex	
Female	1366 (64.86%)
Male	740 (35.14%)
Age (years old)	
Median (range)	57.18 (22~85)
Tumor location	Number (%)
Right upper lobe	800 (38.00)
Right middle lobe	170 (8.10)
Right lower lobe	350 (16.60)
Left upper lobe	512 (24.30)
Left lower lobe	274 (13.00)
Histological subtype	Number (%)
Atypical adenomatous hyperplasia	60 (2.80)
Adenocarcinoma in situ	234 (11.1)
Minimally invasive adenocarcinoma	818 (38.80)
Invasive adenocarcinoma	994 (47.20)
Acinar predominant invasive adenocarcinoma	778 (36.90 total/78.30 within IAC group)
Lepidic predominant invasive adenocarcinoma	56 (2.70/5.60)
Papillary predominant invasive adenocarcinoma	64 (3.00/6.40)
Micropapillary predominant invasive adenocarcinoma	12 (0.60/1.20)
Solid predominant invasive adenocarcinoma	54 (2.60/5.40)
Mucinous adenocarcinoma	30 (1.40/3.00)

papillary predominant invasive adenocarcinoma, 31.25% cases were type I, followed by type II and type VI (both were 18.75%). In addition, half of the cases (50.00%) with micropapillary predominant invasive adenocarcinoma were type II, followed by type III granular lesions (33.34%); types I, IV, V, VI, and VIII were not observed. Type II (59.26%) and type I (22.22%) were solid predominant invasive adenocarcinoma; other types were not observed. Moreover, 40.00% of cases with mucinous adenocarcinoma were type II, 33.33% were type I, and 13.33% were type VII; types IV and VII were not observed.

Discussion

Lung adenocarcinoma may originate in the alveoli, alveolar ducts, respiratory bronchioles, or lobular bronchioles. Different histopathological types of lesions may have different growth and spread speeds. All this may lead to lesions showing different morphological features on CT images. Intratumoral fibrous tissue contraction and traction on the surrounding structures may also contribute to the morphological changes [14–16]. In our study, we analyzed tumor morphological changes as a whole and divided them into eight types and explored the correlation between tumor morphological changes and pathological diagnoses.

Possible pathological correlation for different morphological types of lung adenocarcinomas

Type I (cotton ball): tumor cells grow along the alveolar wall without completely filling the alveolar space, and the alveolar space is not filled by mucus or other fluid. This is often seen in AAH and AIS, consistent with previous studies [8]. These studies have also suggested that MIA and IAC may present as GGNs too, including pGGNs and mGGNs [3, 6]. For mGGNs, small amounts of solid components located in the center and surrounded by GGO can also present cotton ball–like morphology.

Type II (solid fill): the tumor cells or the mucus secreted by the tumor gradually fills up the alveolar space. Meanwhile, the fibrous tissue proliferation gradually increases, and the alveolar structure collapses. The combination of these factors leads to the solid density on CT imaging [15, 17, 18]. mGGNs with higher-density periphery and lower-density centers are also classified as solid fill-type. Type II lesions may develop from cotton ball–type lesions.

Table 2 Solid portion percentage and size of different pathological lesions. The size and the percentage of ground-glass nodule opacities in different pathological types of lesions

Histological subtype	Size (mm)	GGO ratio (%)
Atypical adenomatous hyperplasia	4.38 ± 2.34	100.00 ± 0.00
Adenocarcinoma in situ	5.27 ± 1.90	93.22 ± 15.77
Minimally invasive adenocarcinoma	6.94 ± 3.11	84.36 ± 21.54
Invasive adenocarcinoma	15.34 ± 7.21	41.90 ± 34.39
Acinar predominant invasive adenocarcinoma	15.10 ± 7.18	44.83 ± 34.39
Lepidic predominant invasive adenocarcinoma	15.20 ± 5.39	62.44 ± 24.44
Papillary predominant invasive adenocarcinoma	18.79 ± 7.75	34.64 ± 28.20
Micropapillary predominant invasive adenocarcinoma	18.17 ± 6.58	29.21 ± 38.87
Solid predominant invasive adenocarcinoma	17.12 ± 7.73	9.09 ± 17.40
Mucinous adenocarcinoma	10.33 ± 4.91	7.06 ± 18.03

Table 3 Classification of pre-invasive lesions and early-stage (stage 0 or stage I) lung adenocarcinomas

Group	Classifications							
	Type I	Type II	Type III	Type IV	Type V	Type VI	Type VII	Type VIII
AAH (60)	60 (100%*)	0 (0.00%)	0 (0.00%)	0 (0.00%)	0 (0.00%)	0 (0.00%)	0 (0.00%)	0 (0.00%)
AIS (234)	206 (88.03%)	16** (6.84%)	2 (0.85%)	0 (0.00%)	8 (3.42%)	0 (0.00%)	0 (0.00%)	2 (0.85%)
MIA (818)	696 (85.09%)	54 (6.60%)	14 (1.71%)	10 (1.22%)	14 (1.71%)	6 (0.73%)	2 (0.24%)	22 (2.69%)
IAC (994)	428 (43.06%)	204 (20.52%)	78 (7.85%)	72 (7.24%)	46 (4.63%)	68 (6.84%)	54 (5.43%)	44 (4.43%)
Total	1390	274	94	82	68	74	56	68

* The percentages of different nodule types in each group

** Among 16 cases of type II AIS lesions, seven cases were mucinous subtype

Type III (granular): tumor cells grow along the alveolar space or the bronchiole wall. When the cells fill one or more alveolar sacs, a small solid sphere or bead-like structure is formed, and such a structure in turn appears as one or multiple granules. Alternatively, if discrete parts of the tumor grow faster because of cell differentiations, parts that grow faster can be seen as granules in CT images.

Type IV (dendriform): malignant cells grow along the alveolar duct or bronchus, extend from one to multiple connected alveolar ducts or bronchioles, fill up the ducts, and invade deeper structures. Meanwhile, central fibrosis and resultant tissue contraction can cause thicker fibrotic strands around the tumor with the increased invasiveness of the tumor [19]. All these may contribute to dendriform lesion on CT. Morphology of this type can be better observed with 3D reconstruction than with cross-sectional images.

Type V (bubble-like lucencies): one or more vacuoles or air bronchograms are present in the lesion, and the lesion grows along the cavity wall but does not fully fill the cavities. In patients with emphysema history, lung adenocarcinoma with bubble-like lucencies can be observed. However, the formation of vacuoles and cavities may be attributed to lesion growth too. The cavities referenced in our study were small with thin walls, similar to the bubble-like signs defined by Wu et al [20].

Type VI (honeycomb-like): with the growth of tumor and the proliferation of peripheral tumor cells, central pulmonary scaffold tissues are destructed. This leads to the formation of vacuoles and the formation of larger or polygonal cavities by the merger of multiple vacuoles. Such structural changes give the lesion a honeycomb appearance. Type VI partially overlaps with the bubble-like appearance mentioned in the study by Saito et al [21], since both of them have inflated bronchi, irregular shape, pleural indentation, and other similar features.

Table 4 Morphological classification for different subtypes of invasive adenocarcinoma

Subtype	Morphological classification of nodules							
	I	II	III	IV	V	VI	VII	VIII
Acinar (778)	350 (45.0%*)	140 (18.00%)	54 (6.94%)	62 (7.97%)	36 (4.63%)	50 (6.43%)	46 (5.91%)	40 (5.14%)
Lepidic (56)	34 (60.71%)	2 (20.52%)	8 (14.29%)	0 (0.00%)	4 (7.14%)	4 (7.14%)	2 (3.57%)	2 (3.57%)
Papillary (64)	20 (31.25%)	12 (18.75%)	10 (15.63%)	6 (9.38%)	2 (3.13%)	12 (18.75%)	0 (0.00%)	2 (3.13%)
Micropapillary (12)	0 (0.00%)	6 (50.00%)	4 (33.34%)	0 (0.00%)	0 (0.00%)	0 (0.00%)	2 (16.67%)	0 (0.00%)
Solid (54)	14 (25.93%)	32 (59.26%)	0 (0.00%)	4 (7.41%)	0 (0.00%)	2 (3.70%)	2 (3.70%)	0 (0.00%)
Mucinous (30)	10 (33.33%)	12 (40.00%)	2 (6.67%)	0 (0.00%)	4 (13.33%)	0 (0.00%)	2 (6.67%)	0 (0.00%)
Total	428	204	78	72	46	68	54	44

* The percentages of different nodule types in each group

Type VII (scar-like): the lesion originates from intrinsic scar tissues. It overlaps with the formerly defined scar cancer. The scar tissues may be secondary to tuberculosis, bronchiectasis, pulmonary abscess, organized pneumonia, trauma, or infarction. The tumor then develops from existing scar tissues [14, 22]. Although the entire lesion can be large, the tumor component can be limited, appearing solid or as GGO on CT image [23].

Type VIII (notched or umbilication): when the tumor is located near the interlobular pleura, the fibrous tissue proliferation stimulated by the tumor may contract, leading to pleural thickening, adhesion, and notched appearance. If there are existing linear fibrous tissues near a less invasive tumor, then tumor growth may be limited in parallel to the fibrous tissue, resulting in local contraction which forms notches. Type VIII is different from pleural indentation. Typical pleural indentation is caused by the traction from the tumor, and there is no thickening or adhesion of the local pleura [24]. For type VIII appearance, local adhesion or pleural thickening can occur.

Relationships between morphological and pathological features in pre-invasive lesion and early-stage lung adenocarcinoma

Our data indicates that different morphological classifications correlate to different pathological types ($p < 0.05$). Type I was the most common morphological type in AAH, AIS, MIA, and IAC; however, the percentage of type I gradually decreased with tumor progression. The percentage of solid component was also correlated with the morphological classification. For pGGNs, the manifestations of such lesions had mostly type I cotton ball appearance. All AAHs in our study were pGGN and manifested as type I. AIS and AAH were both pre-invasive lesions. AIS was further divided into non-mucinous and mucinous subtypes. The mucinous subtype can secrete mucus that fills up the alveolar cavity and may manifest as solid nodule on CT. In this study, seven cases (7/234) of AIS were mucinous subtype, along with nine cases of non-mucinous AIS showing type II lesions.

For invasive adenocarcinoma, mGGN can be seen with localized clusterings of tumor cells, localized invasions, alveolar wall collapses, or tumor-stimulated fibrous tissue proliferation. The size of invasion is not the only pathological diagnostic criterion for IAC. The following situations are also defined as invasion: (1) all histological subtypes other than lepidic subtype (e.g., acinar, papillary, micropapillary, and solid subtypes) and (2) the presence of myofibroblast cell matrix related to invasive tumor cells [8]. In the latter two scenarios, tumor growth-related density increase may not manifest as solid components in CT; therefore, IAC can also appear as pGGN or mGGN in CT images, and thus it can be classified as type I lesions. MIA and IAC are both considered invasive adenocarcinomas, where MIA is an early-stage IAC. In our study, MIA often (85.09%) manifested as type I cotton ball lesions. Among MIAs, 54 (6.60%) cases presented as solid lesions; other morphological types were also found, but with lower percentages. Among the IAC patients, 428 (43.06%) cases showed type I lesions; 204 (20.52%) cases showed type II lesions, and the other morphological types were evenly distributed, with percentages higher than MIA.

Among the pathological subtypes of stage I IAC, most of the cases (78.27%) were acinar predominant invasive adenocarcinoma, and they may manifest as different morphological types because of the larger sample size. The data obtained in our study revealed that micropapillary predominant invasive adenocarcinoma, solid predominant invasive adenocarcinoma, and mucinous adenocarcinoma mostly manifested as type II (solid fill) morphology, while acinar predominant invasive adenocarcinoma, lepidic predominant invasive adenocarcinoma, and papillary predominant invasive adenocarcinoma mostly manifested as type I (cotton ball) morphology. Previous study has shown that among invasive adenocarcinomas, the prognosis is worse for micropapillary predominant and solid predominant adenocarcinomas with mucin production [25]. These results suggested that morphological classifications and pathological subtypes of lung adenocarcinoma and patient prognosis may be correlated. According to the new classification of lung adenocarcinoma published in 2011, for the subtypes of invasive adenocarcinomas, the percentages of histological types should be recorded in 5% increments, not simply recorded by the primary type [8]. In our study, we listed the main pathological subtypes of invasive adenocarcinoma according to the highest percentages. The morphological classification in different pathological subtypes of invasive adenocarcinoma needs future studies.

While some of the morphological types can be easily distinguished (e.g., type I, type III, and type VII), others may be hard to differentiate (e.g., type VI and type IX). Previous imaging data may help the classification, e.g., lesions developed from existing scars are of type VII. In addition, the morphological classifications and pathological subtypes are not in a one-to-one relationship. Some morphological types are mutually exclusive. For example, if the lesion is a type I cotton type, then it cannot be type III granular type. But morphological types can also co-exist. For example, if lung adenocarcinoma is located near the interlobular pleura, it can show typical umbilicated appearance and also have small cavities inside the lesion. In our study, such lesions were classified as type VIII notched or umbilication, but they also can be classified as type V bubble-like lucencies.

Several potential limitations of this study should be noted. Because only two radiologists evaluated the images, certain deviations in the results might be caused by subjective morphological diagnosis. In addition, the image features were not accurately compared with pathological changes. Such comparison will be done in future studies.

In conclusion, by categorizing pre-invasive lesions and early-stage lung adenocarcinoma into eight morphological types, it is possible to gain a better understanding of the overall morphological characteristics and improve pre-surgical diagnosis and differential diagnosis.

Acknowledgements I would like to express my gratitude to all those who helped me during the writing of this paper.

Funding This study has received funding by the Research Program of Shanghai Hospital Development Center (SHDC22015025) and the Medical Imaging Key Program of Wise Healthcare Technology 120, Health Commission of Shanghai (2018ZHYL0103).

Compliance with ethical standards

Guarantor The scientific guarantor of this publication is Ming Li.

Conflict of interest The authors of this manuscript declare no relationships with any companies, whose products or services may be related to the subject matter of the article.

Statistics and biometry No complex statistical methods were necessary for this paper.

Informed consent Written informed consent was waived by the Institutional Review Board.

Ethical approval Institutional Review Board approval was obtained.

Study subjects or cohorts overlap Some study subjects or cohorts have been previously reported in "*CT features of lung scar cancer*". J Thorac Dis 2015;7(3):273–80.

Methodology
- retrospective
- diagnostic/observational
- performed at one institution

References

1. Torre LA, Bray F, Siegel RL, Ferlay J, Lortet-Tieulent J, Jemal A (2015) Global cancer statistics, 2012. CA Cancer J Clin 65(2):87–108
2. Chen F, Cole P, Bina WF (2007) Time trend and geographic patterns of lung adenocarcinoma in the United States, 1973–2002. Cancer Epidemiol Biomarkers Prev 16(12):2724–2729
3. Zhang Y, Shen Y, Qiang JW, Ye JD, Zhang J, Zhao RY (2016) HRCT features distinguishing pre-invasive from invasive pulmonary adenocarcinomas appearing as ground-glass nodules. Eur Radiol 26(9):2921–2928
4. Wu F, Tian SP, Jin X et al (2017) CT and histopathologic characteristics of lung adenocarcinoma with pure ground-glass nodules 10 mm or less in diameter. Eur Radiol 27(10):4037–4043
5. Gao F, Sun Y, Zhang G, Zheng X, Li M, Hua Y (2018) CT characterization of different pathological types of subcentimeter pulmonary ground-glass nodular lesions. Br J Radiol:20180204
6. Mao H, Labh K, Han F, Jiang S, Yang Y, Sun X (2016) Diagnosis of the invasiveness of lung adenocarcinoma manifesting as ground glass opacities on high-resolution computed tomography. Thorac Cancer 7(1):129–135
7. Goldstraw P, Chansky K, Crowley J et al (2016) The IASLC lung cancer staging project: proposals for revision of the TNM stage groupings in the forthcoming (eighth) edition of the TNM classification for lung cancer. J Thorac Oncol 11(1):39–51
8. Travis WD, Brambilla E, Noguchi M et al (2011) International association for the study of lung cancer/American thoracic society/European respiratory society international multidisciplinary classification of lung adenocarcinoma. J Thorac Oncol 6(2):244–285
9. Kim HY, Shim YM, Lee KS, Han J, Yi CA, Kim YK (2007) Persistent pulmonary nodular ground-glass opacity at thin-section CT: histopathologic comparisons. Radiology 245(1):267–275
10. Henschke CI, Yankelevitz DF, Mirtcheva R, McGuinness G, McCauley D, Miettinen OS (2002) CT screening for lung cancer: frequency and significance of part-solid and nonsolid nodules. AJR Am J Roentgenol 178(5):1053–1057
11. Ko JP (2005) Lung nodule detection and characterization with multi-slice CT. J Thorac Imaging 20(3):196–209
12. Aoki T, Tomoda Y, Watanabe H et al (2001) Peripheral lung adenocarcinoma: correlation of thin-section CT findings with histologic prognostic factors and survival. Radiology 220(3):803–809
13. Madri JA, Carter D (1984) Scar cancers of the lung: origin and significance. Hum Pathol 15(7):625–631
14. Nambu A, Araki T, Taguchi Y et al (2005) Focal area of ground-glass opacity and ground-glass opacity predominance on thin-section CT: discrimination between neoplastic and non-neoplastic lesions. Clin Radiol 60(9):1006–1017
15. Winer-Muram HT (2006) The solitary pulmonary nodule. Radiology 239(1):34–49
16. Gao F, Li M, Ge X et al (2013) Multi-detector spiral CT study of the relationships between pulmonary ground-glass nodules and blood vessels. Eur Radiol 23(12):3271–3277
17. Lee HY, Lee KS, Han J et al (2009) Mucinous versus nonmucinous solitary pulmonary nodular bronchioloalveolar carcinoma: CT and FDG PET findings and pathologic comparisons. Lung Cancer 65(2):170–175
18. Gaeta M, Vinci S, Minutoli F et al (2002) CT and MRI findings of mucin-containing tumors and pseudotumors of the thorax: pictorial review. Eur Radiol 12(1):181–189
19. She Y, Zhao L, Dai C et al (2017) Preoperative nomogram for identifying invasive pulmonary adenocarcinoma in patients with pure ground-glass nodule: a multi-institutional study. Oncotarget 8(10):17229–17238
20. Wu F, Cai ZL, Tian SP et al (2015) Correlations between pathologic subtypes/immunohistochemical implication and CT characteristics of lung adenocarcinoma ≤ = 1 cm with ground-glass opacity. Zhongguo Yi Xue Ke Xue Yuan Xue Bao 37(2):163–170
21. Saito H, Yamada K, Hamanaka N et al (2009) Initial findings and progression of lung adenocarcinoma on serial computed tomography scans. J Comput Assist Tomogr 33(1):42–48
22. Bobba RK, Holly JS, Loy T, Perry MC (2011) Scar carcinoma of the lung: a historical perspective. Clin Lung Cancer 12(3):148–154
23. Gao F, Ge X, Li M et al (2015) CT features of lung scar cancer. J Thorac Dis 7(3):273–280
24. Yang X, Soimakallio S (1997) Pleural signs of small peripheral pulmonary masses: pathologic correlation with chest radiographs and diagnostic value. Eur J Radiol 25(2):146–151
25. Yoshizawa A, Motoi N, Riely GJ et al (2011) Impact of proposed IASLC/ATS/ERS classification of lung adenocarcinoma: prognostic subgroups and implications for further revision of staging based on analysis of 514 stage I cases. Mod Pathol 24(5):653–664